



Article

An Automatic Approach to Extracting Large-Scale Three-Dimensional Road Networks Using Open-Source Data

Yang Chen ^{1,2,3} , Xin Yang ^{1,2,3,*}, Ling Yang ^{1,2,3} and Jiayu Feng ⁴¹ School of Geography, Nanjing Normal University, Nanjing 210023, China² Key Laboratory of Virtual Geographic Environment, Nanjing Normal University, Ministry of Education, Nanjing 210023, China³ Jiangsu Center for Collaborative Innovation in Geographical Information Resource Development and Application, Nanjing 210023, China⁴ School of Architecture and Urban Planning, Huazhong University of Science and Technology, Wuhan 430074, China

* Correspondence: xxinyang@njnu.edu.cn

Abstract: 3D road networks are amongst the indispensable elements of a smart city, which has been explored in various ways. However, researchers still faces challenges extracting 3D networks on a large scale. The global digital surface models (DSMs) with relatively high spatial resolution make it possible to extract 3D road networks. Nevertheless, the complete and accurate elevation of road networks cannot be obtained directly because of the limitation in sensors on the DSM production platform. Thus, we proposed a novel approach to extract large-scale 3D road networks, integrating terrain correction and road engineering rule constraint, by using the Advanced Land Observing Satellite World 3D-30 m DSM, OpenStreetMap and FABDEM. The simplification and terrain correction algorithm were applied to remove most of the edges with excessive grades and reduced the negative impact of the built-up environment in DSM on the extraction accuracy. Moreover, the tunnel parts of the 3D road networks were refined based on road engineering standards. Nanjing of China, Aalborg of Denmark and Los Angeles of the United States are selected as study areas. Using 3D road networks from unmanned aerial vehicle photogrammetry, light detection and ranging and Google Earth as references, we validated the road elevation accuracy of our method and obtained an overall root-mean-square error of 3.80 m and a mean absolute error of 1.94 m. The 3D topology of interchanges with different radii was reconstructed completely. Overall, our work is an endeavour to utilise multiple open-source data to extract large-scale 3D road networks and benefits future research related to smart city reconstruction and 3D urban analysis.

Keywords: 3D road networks; FABDEM; AW3D30 DSM; OSM

Citation: Chen, Y.; Yang, X.; Yang, L.; Feng, J. An Automatic Approach to Extracting Large-Scale Three-Dimensional Road Networks Using Open-Source Data. *Remote Sens.* **2022**, *14*, 5746. <https://doi.org/10.3390/rs14225746>

Academic Editors: Gavin McArdle, Mir Abolfazl Mostafavi and Hamidreza Rabiei-Dastjerdi

Received: 23 September 2022

Accepted: 11 November 2022

Published: 14 November 2022

Publisher's Note: MDPI stays neutral with regard to jurisdictional claims in published maps and institutional affiliations.



Copyright: © 2022 by the authors. Licensee MDPI, Basel, Switzerland. This article is an open access article distributed under the terms and conditions of the Creative Commons Attribution (CC BY) license (<https://creativecommons.org/licenses/by/4.0/>).

1. Introduction

Urban road networks are expanding rapidly due to the rapid urbanisation worldwide, especially in developing countries, such as China [1]. As the skeleton of cities, urban road networks play a significant role in analysing the accessibility of public infrastructure [2], predicting traffic congestion [3,4] and exploring the jobs–housing relationship [5]. Owing to the surge of population and the tight land supply, urban traffic problems are gradually coming to the fore [6]. To relieve the traffic pressure, most cities have adopted the solution of building 3D road entities, including overpasses and tunnels, especially at transportation hubs [7]. However, most urban analyses are based on 2D urban road networks without considering the verticality of the urban road networks [8–11].

Within the context of real 3D modelling and digital twins, 3D road networks, an essential part of 3D entities, are constantly being reconstructed [12,13]. In the study of vehicle navigation, multilevel road networks, such as grade-separated interchanges and elevated roads, have been increasingly used to improve navigation accuracy [14]. As a key

element of the 3D structure of a city, similar to buildings, 3D road networks also indicate the stage of urban expansion [15]. Moreover, 3D road networks can be applied to accurately predict fuel consumption [16,17]. Therefore, the verticality of road networks has become an essential topic in urban studies.

There are various approaches for acquiring the elevation of 3D road networks. We divide the elevation information of roads into direct and indirect categories in accordance with the acquisition method. Direct acquisition means the direct measurement of the elevation of points using surveying instruments or tools, such as real-time kinematics [18] and light detection and ranging (LiDAR) [19–21]. In the conventional production process, road surveyors used to measure elevation information and manually interpolate 3D models, which is time consuming and costly. Gao extracted 3D roads with satisfactory results by integrating LiDAR point clouds and high-resolution remote sensing imagery in Hong Kong [22]. Airborne laser scanning is also widely used to reconstruct highway 3D models in multiple terrain areas, which performs well but is limited by the policies in some regions [23]. Although these methods ensure high accuracy, they require high labour and equipment costs and a complicated solving process. Therefore, these methods cannot cope with large-scale tasks. Various data with elevation information, such as digital elevation models (DEMs), digital surface models (DSMs) and crowd-sourced moving trajectory data, are the main indirect ways to obtain large-scale elevation data [24–26]. Wang utilised high-resolution DEM and road centrelines to model high-fidelity roads [27]. Nonetheless, this approach focused on road modelling rather than the accuracy. Schpok extracted city-wide elevated road structures by using high-resolution DSMs. Though he designed an algorithm against noise in DSM elevations, this approach still relies heavily on the precision of the DSM [28]. McKenzie presented a radical approach by deriving road network elevation data from massive amounts of in situ observations extracted from crowd-sourced moving trajectory data [24]. However, obtaining a considerable amount of trajectory data requires a large number of users as support, and most researchers cannot obtain such data and cover the cost. Additionally, some large-scale 3D urban road network data come from government departments, and some enterprises pay for services, such as Google Map API [29] or a planning department's dataset. Generally, obtaining such data has a financial cost, and their accuracy, reliability and timeliness cannot be fully guaranteed.

Although some high-resolution DEMs or DSMs produced by unmanned aerial vehicles (UAVs) have a high level of precision, they cannot be applied to extract valid 3D road networks for large-scale regions [30]. Most of the DEM datasets, including SRTM and Advanced Spaceborne Thermal Emission and Reflection Radiometer Global DEM (ASTER GDEM), provide elevation data sources with 30 m (1 arc second) or 90 m (3 arc seconds) spatial resolution and coverage of most of the world, which meet the needs of large-scale studies [31,32].

Several studies have employed the above open-source DEMs as elevation data sources to extract 3D road networks for relatively large regions. Zhang proposed a template-based method to tackle the challenges of generating a large-scale virtual road network environment based on DEM [33]. SRTM was utilised in the reconstruction of 3D city models, including roads from OpenStreetMap (OSM) in Germany [34]. Integrating satellite imagery and semantic information, Wang segmented the elevation data into intersections and generated the surface of the 3D road network on a large scale [35].

Nevertheless, DEM, a discrete mathematical representation of the earth's surface topography [36], does not contain the elevation information of 3D road structures, such as viaducts and interchanges in cities. Meanwhile, DSM generally refers to the land surface model that contains the heights of buildings and trees [37]. In unprocessed DSMs, we can recognise the approximate morphology of viaducts and interchanges with visual interpretation, which shows that DSMs contain 3D road structures and lay the foundation for the subsequent extraction work. Notably, the Advanced Land Observing Satellite (ALOS) World 3D-30 m (AW3D30) DSM and Copernicus DEM (a new DSM rather than

DEM) cover most areas of the world with high accuracy [38,39]. These characteristics indicate that using DSMs is an alternative to extract large-scale 3D road networks.

The extraction of 3D roads by using such DSMs as AW3D30 DSM and Copernicus DEM still faces many challenges. The elevations of urban roads are influenced by other urban entities, such as surrounding buildings and trees. Although the AW3D30 DSM and Copernicus DEM have different instrument types, these entities both interfere with signals and have a negative impact on the vertical precision of DSM in urban heterogeneous areas, due to shadowing and obscuring effects [40,41]. Rugged and complex terrain conditions make sensors incorrectly estimate road surface elevation in some urban regions, even if DSMs have been corrected by fusing multisource data. Furthermore, given that most DSMs are produced by photogrammetry or synthetic aperture radar (SAR), the bands of their sensors fail to penetrate urban canopies in most cases and only obtain the surface elevation [28]. Therefore, DSMs lack the complete elevation of tunnels and grade-separated interchanges, which are essential parts of 3D road networks.

In summary, there are three issues that are worth noting. (1) The methods for local 3D road network extraction and modelling fail to meet the demand of large-scale 3D road network datasets. (2) Related works tried to extract large-scale 3D roads through original DSMs or DEMs, but ignored the negative impacts of built-up environments on sensors and led to bias in high-rise buildings regions. (3) interchanges and tunnels are essential parts of a 3D road structure, but the methods for large-scale networks failed to reconstruct them because the sensors of DEMs or DSMs are unable to penetrate urban surfaces and their results lacked the complete information of 3D transportation facilities, e.g., interchanges, tunnels and viaducts.

2. Data

2.1. OSM

OSM, a website offering globally renowned volunteered geographic information, aims to provide users with free and easily accessible digital map resources, including site types, building footprints, roads and other geographic information, and has been widely used in urban planning, GIS and other related fields of research [42–44]. OSM roads can be converted into a complete directional network consisting of nodes and edges. Various semantic attributes, such as road type and maximum road speed, are integrated into attribute tables. Users can download the recently updated OSM urban road 2D network for free from the OSM website or through the OSMnx tool, compared with other road datasets released by government departments [45]. Therefore, the OSM road network is used in this study.

2.2. AW3D30 DSM

ALOS AW3D30 DSM data are derived from the DSM dataset, publicly released by the Japan Aerospace Exploration Agency. The data were obtained by observing and processing the global land area at about 80 degrees north and south latitude by the PRISM stereo camera onboard the ALOS, with a horizontal resolution of 30 m and a vertical accuracy of 5 m [46,47].

Owing to the fusion of multiple data sources, the coverage of AW3D30 DSM data is greater than that of SRTM and Copernicus DEM. Previous studies have shown that the vertical accuracy of AW3D30 DSM is better than that of SRTM and ASTER GDEM [38]. Moreover, AW3D30 has been widely used in related research areas, including building height extraction [48], topographic analysis of landslides [49] and landform classification mapping [50], with good results. These characteristics indicate that it is reliable regarding vertical accuracy and is an excellent elevation data source for extracting 3D road network elevations.

2.3. FABDEM

FABDEM is a 30 m-spatial resolution global DEM dataset without buildings and forests, produced using machine learning methods from Copernicus DEM [51]. As a reference, Copernicus DEM has good performance in vertical accuracy and newer production time [52]. Compared with other DEMs, it retains more realistic surface elevation information and fits the urban terrain surface more accurately, which contributes to calculating essential urban terrain factors, such as slope and aspects. Figure 1 illustrates how FABDEM removes most of the noise from urban areas, including buildings and trees, and shows the natural terrain surface of the urban areas.

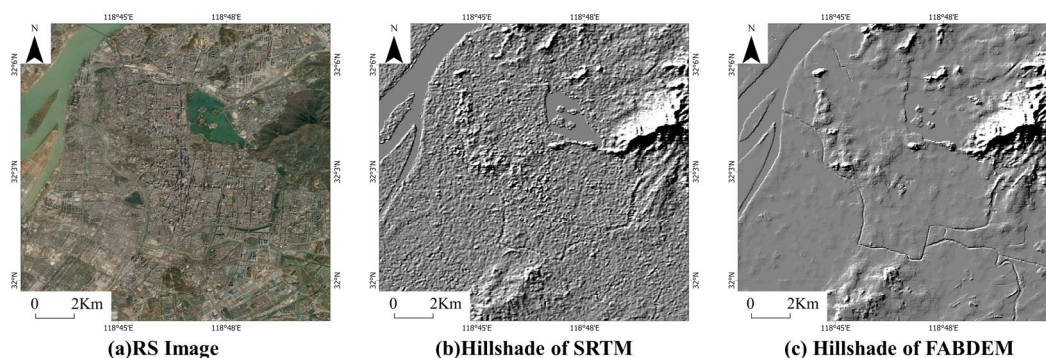


Figure 1. A comparison of the hillshade effect of SRTM (b) and FABDEM (c) with reference to (a) Remote sensing images in the central area of Nanjing.

3. Method

We propose a novel 3D road network extraction method considering terrain correction and construction rule constraints. Figure 2 illustrates the workflow for extracting 3D road networks from multiple open-source data, which consists of three steps.

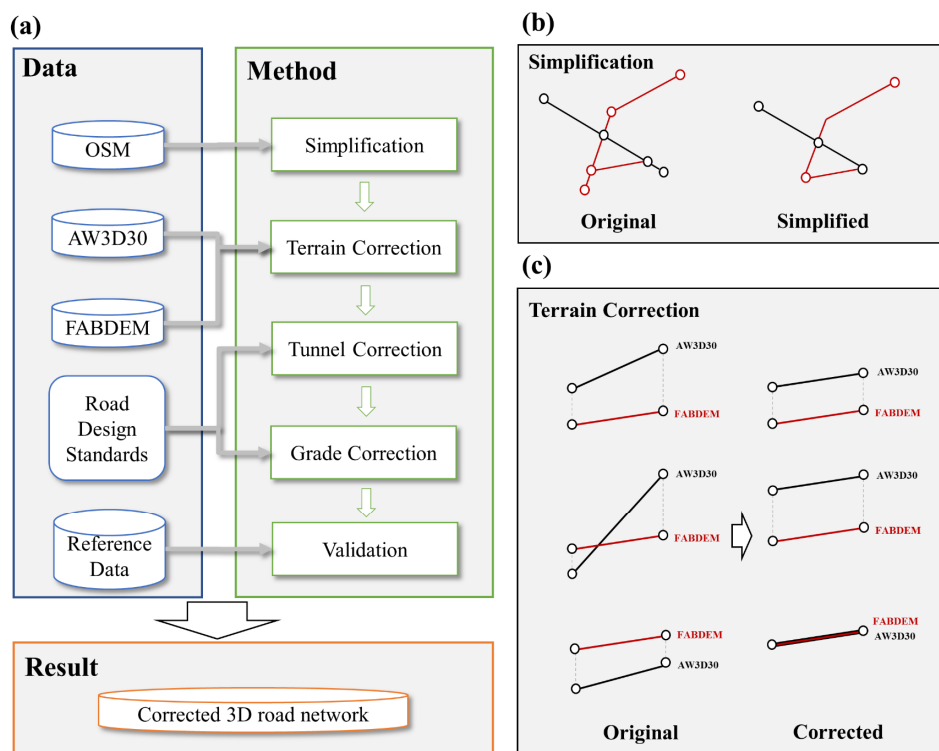


Figure 2. (a) Workflow diagram for extracting 3D road networks, (b) The detailed process of simplification, (c) The detailed process for terrain correction.

The first section utilises topological features and road attribute information to simplify the OSM road nodes. It is followed by terrain correction based on FABDEM data to reduce the effect of terrain noise in AW3D30 DSM on road elevation. Then, the road engineering construction standards applied to reconstruct road segments, such as tunnels. On this basis, we fix the rest of the roads with excessive grade as much as possible to make the undulation level of 3D roads closer to the actual situation. Finally, we use the corrected data to verify the accuracy of the estimation results from the aspects of elevation and topology by using the reference 3D road network data. All the elevation extraction work is performed for the nodes in the road network, and for the other locations in the roads (non-node locations) it is accomplished by linear interpolation between two nodes. Many roads within residential roads and living streets in the OSM data are not included in our study because of the limitation in DSM resolution.

3.1. Simplification

The OSM road network consists of nodes and edges, where each node is usually a topological feature point in its road segment. Specifically, nodes can be used to define standalone point features but are more commonly used to determine the shape or path of a road [53]. Figure 3 shows the original result from DSM, with the 3D building information added. The yellow rectangular boxes illustrate the obviously wrong nodes, which are mainly located around high-rise buildings. We speculate that the surrounding buildings, the ground railroad and similar entities have a negative impact on the sampling of several nodes, due to shadowing and obscuring effects. Thus, confirming suitable sampling points is a key to road elevation extraction.

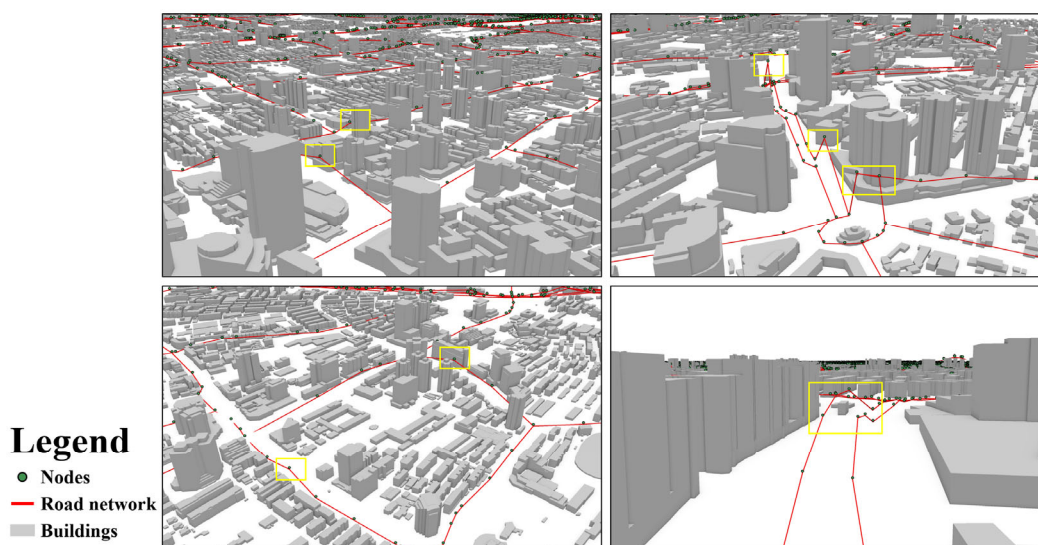


Figure 3. The original networks and errors with 3D building in urban areas.

Generally, the points of the intersections are not only well open but are far away from buildings, trees and other objects, so that the sensors of satellites are influenced by buildings and trees and make more accurate measurements of the road surface elevation. With reference to the principle of vertical road planning, the trend of grades remains the same between two road intersections in a segment. Specifically, the elevation of other nonintersecting points takes a range between the values of the intersection. Thus, based on the potential influencing factors and principle of vertical road planning, we simplify the topology of the entire network by removing nonintersecting points or dead ends (Figure 2b), which merges short road segments into one between two intersections and reduces the influence of buildings and trees. By converting the road networks to undirected graph, the degrees of nodes are calculated. And the nodes with a degree greater than 3 are considered

as intersections and the others are filtered. To accomplish this graph-related task, we import the NetworkX [54] package into our python program.

A number of simplified nodes are usually obscured by the upper roads in interchanges, and sensors fail to penetrate the upper roads, which leads the elevation of these nodes to represent the surface of upper roads as a type of noise in DSM. Whilst the nodes of lower roads in interchanges are simplified, the nodes in the intersections of ramps and roads are reserved. The reserved nodes not only have better measurement conditions than other nodes but are also the key points in the topology of the interchanges. After simplification, the lower roads in the interchanges only reserved two nodes, which are accurate in the original DSM. Thus, these roads, floating in the air, are corrected to the lower location of the interchanges. Using these reserved nodes, we can eliminate considerable noise and reconstruct the interchanges. The number of nodes is significantly reduced (Figure 4) based on the rules, which would help us to improve the performance of the workflow.



Figure 4. A comparison of simplified nodes and original nodes in the central area of Nanjing.

3.2. Correction

Three steps in sequence, namely, terrain correction, tunnel correction and grade correction, are conducted to minimise the cases in which errors exist in data. We disregard the connecting road segments, such as ramps and auxiliary roads, in our correction work because the width of connecting roads is usually much smaller than the size of pixels and is hardly represented in global DSMs. In comparison, major roads are more easily detected by sensors, and their result contains less noise. Thus, we use interpolation to obtain the elevation of connecting road segments from two adjacent intersections of major roads but not road length limit.

3.2.1. Terrain Correction

In the previous study, we found that the elevations of some nodes in the AW3D30 DSM data are underestimated at high values and overestimated at low values [48]. Urban land surface would be lower than DSM in most built-up areas in our perspectives. To verify it, we use the results of AW3D30 DSM minus FABDEM via the Raster Calculator in ArcGIS

to assess it. The result is reclassified into four categories, where the warm tones represent areas where the elevation of DSM is greater than that of DEM, and the opposite applies for cool tones. Figure 5 shows that the elevation values of AW3D30 DSM are greater than those of FABDEM in most pixels, whilst the minus values are generally found in such locations as rivers and lakes. According to visual interpretation, the values of AW3D30 DSM in most road segments are slightly greater than those of FABDEM, but a huge difference is found in building areas. Given that AW3D30 DSM has been evaluated worldwide and obtained good accuracy, the outcomes by our raster calculation indicate that FABDEM is suitable as a land surface elevation data source of AW3D30 DSM.

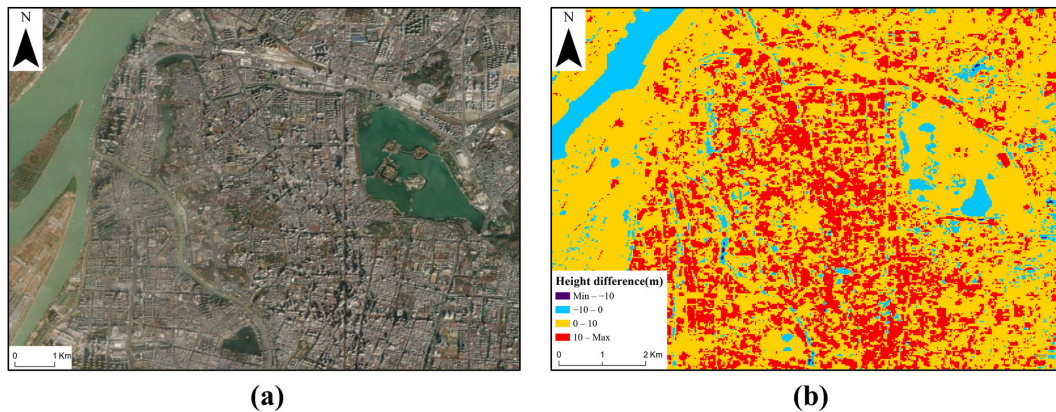


Figure 5. (a) RS image, (b) Result of AW3D30 minus FABDEM.

The grades in the DEM are relatively plausible because the DEM represents the land surface elevation without any other objects, and the grades of artificially constructed roads are generally not greater than those in the DEM. However, some areas are opposite. To cope with it, we develop a correction workflow that if the absolute value of the grade between two nodes on the DSM is greater than the grade on the DEM, then the elevation of a node in the two nodes is considered unreliable. In response, the elevations of the original untrustworthy nodes are recalculated using the grade of the DEM with the elevation of the trustworthy node.

There are three situations that require terrain correction. Figure 2c indicates the problems and our correction workflow. (1) The DSM values of both nodes are higher than the DEM values because the values of DSM are easily influenced by noise information, such as high-rise buildings, trees and above-ground railroads, which will cause their elevation to be significantly overestimated from the DEM values and other non-noise nodes. These pair nodes are main noise in the original data. Thus, we reserve the elevation of the lower node and use the grade of DEM to recalculate the elevation of the upper node instead of the grade of DSM. (2) When only one of the pair nodes is greater than the DEM value, the lower nodes are not credible because the road would be built based on the original land surface and not lower than the FABDEM. Therefore, we use the values of DEM to replace the elevation of lower nodes and recalculate the grades of these road segments. (3) If the elevations of two nodes are lower than the DEM values, then the values of DEM would be considered the elevations of the nodes.

Based on the rules above, these nodes are corrected by land surface, and the correction values corresponding to each node are stored as a list. Given that the same node is connected to several nodes in road segments, the elevation values obtained from the correction work inherit the elevation and terrain information from the different nodes. Choosing a correct value from many candidate values is important. The previous step eliminates some noise, but the remaining noise would influence the result accuracy, especially when the absolute grades are greater than the original DEM. Considering that the nodes may inherit or exaggerate noise, when the number of candidate corrected values is greater than two, we select the combination with the smallest intra-group variance in the candidate values and

calculate the mean value within its minimum variance group as its final terrain correction elevation value. If the number of candidate values is less than or equal to two, we calculate the mean of values as result directly. This step is helpful to filter the noise from the candidate values.

3.2.2. Tunnel Correction

Given that AW3D30 DSM is a product of photogrammetry, the sensors cannot completely detect the essential parts in a 3D road network, especially tunnels. Thus, the correction for tunnels is performed based on the previous simplification and terrain correction. We check the tunnel construction standard adopted and published by the American Association of State Highway and Transportation Officials in the USA [55] and determine that the minimum height of tunnels cannot be lower than 14 feet, i.e., 4.26 m. Though the technical standard for highway engineering in urbanised areas (JTG 2112–2021) issued by the Chinese Ministry of Transportation [56] does not specify the height limitation for tunnels, it states that for expressways, first-class roads and other high-level roads, the height limit for vehicles is 5 m, and that for the other road segments is below 5 m. Considering the regional variability of this criterion and global suitability of our approach, we combine the two standards and calculate the mean tunnel height. To facilitate the calculation, the tunnel height was set to 4.5 m generally. In our software, users could modify this variant for local urban cases and standards. Through OSM, we can quickly query tunnel sections' distribution by road data attributes. Based on the result of the previous workflow, the elevation of the nodes at each end identified as tunnel sections is lowered by 4.5 m. Figure 6 shows the detailed process for the tunnel correction process. As a result, the original tunnel nodes over the terrain surface were corrected to below the ground and the tunnel sections were reconstructed.

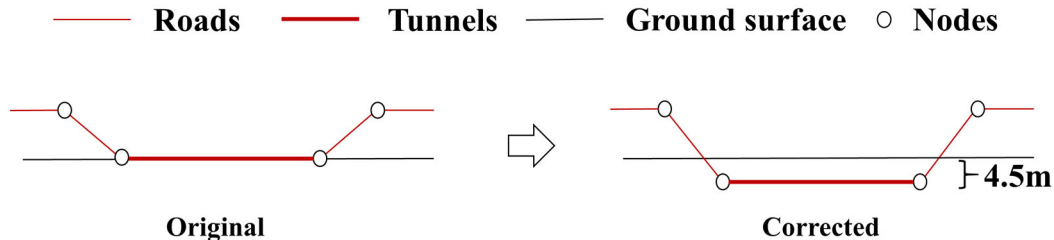


Figure 6. The detailed process for the tunnel correction process.

Though tunnel correction may exaggerate the structure of tunnel sections and sacrifice some accuracy, this workflow reconstructs various tunnel patterns in the 3D road network, fixes the problem of missing tunnel sections in the original dataset and improves the completeness of the entire network.

3.2.3. Grade Correction

Despite completing the terrain correction and tunnel correction, minimal noise remains in the 3D road network. We find that a small number of edges connected by these noisy nodes still have the characteristics of excessive grades. According to the requirements of road grades mentioned in the highway design manual from CA (Table 1) [57] and JTG 2112–2021 (Table 2), the grade standards relate to the road design speed and terrain situations. Our method mainly focuses on tertiary and higher-level roads. Most cities with tertiary roads are generally distributed in the plain or rolling areas [48], which means the roads are not very steep. Additionally, according to standards of CA and JTG 2112–2021, the design speed of tertiary roads is between 30–60 km/h and high-level roads have greater designed speed, so we take 0.07 as the maximum grade.

Table 1. Maximum grades for types of highway and terrain conditions.

Type of Terrain	Freeways and Expressways	Rural Highways	Urban Highways
Level	3%	4%	6%
Rolling	4%	5%	7%
Mountainous	6%	7%	9%

Table 2. Maximum grades for types of roads in JTG 2112–2021.

Designed Speed (km/h)	Maximum Grades (%)
120	3
100	3
80	4
60	5
50	5.5
40	6
30	7
20	8

For the entire urban 3D road network, if the grade of one edge is greater than the value of 0.07, then this edge is not credible and should be corrected. To solve it, we reduce the elevation value of the untrustworthy node to the value of the other node in an edge and repeat the previous operation until all the untrustworthy edges are traversed.

In the whole correction step, we realise simplification and terrain correction to reduce the influence of the systematic error of AW3D30 DSM data on the elevation. On this basis, we develop a series of rules through the expert knowledge from American road construction standards and Chinese road engineering specifications. As a result, masses of the noise are removed from the urban 3D road network. Some road segments, such as interchanges, tunnels and approach roads that are reconstructed, so that the overall road network is more in line with road engineering specifications.

3.3. Validation with Reference Data

Three cities in three continents, namely, Nanjing of China, Aalborg of Denmark and Los Angeles of the USA, are selected for validation. In the validation process, we use random sampling of some nodes to calculate the bias. Root-mean-square error (RMSE) and mean absolute error (MAE) are widely applied to measure deviations between predicted and reference values, which are also used to evaluate the model performance by the following equations.

As a supplement, we further combine remote sensing images to sample three classical interchanges to check the 3D topological correctness. In the topology assessment of the road network, we plan to verify the relative location of ramps and main roads in the interchanges by visual interpretation.

$$RMSE = \sqrt{\frac{\sum_{i=1}^n (h_{e,i} - h_{r,i})^2}{n}} \quad (1)$$

$$MAE = \frac{\sum_{i=1}^n |h_{e,i} - h_{r,i}|}{n} \quad (2)$$

where $h_{e,i}$ corresponds to the elevation value of the corrected node i , $h_{r,i}$ corresponds to the elevation value of the reference node i , and n represents the total number of nodes.

4. Result

4.1. Accuracy Assessment of Road Network Elevation

Three sample areas distributed across three continents with different data sources are used to evaluate the accuracy of the 3D road network elevations. These three cities have

different levels of population and diverse patterns of road networks. Based on previous classifications, their road network patterns are mixed, sphere and grid, respectively [58], which make our validation more representative. A high-resolution DSM has been processed in our previous work, and the spatial resolution is about 0.03 m in Nanjing from UAVs. Considering that these high-resolution data still contain much noise, including trees and streetlamps, the DSM data was repaired by comparing them with remote sensing images. For Aalborg, we refer to the LiDAR data published by Aarhus University, which have a nominal accuracy of plus or minus 20 cm [20]. Google Earth is known to provide accurate 3D models and elevation data in most parts of the world, so our study samples 200 points in Los Angeles to compare and verify with it. These areas comprise tunnels, interchanges and other 3D traffic projects, which are very representative in complex urban environment.

In Nanjing, 279 sampling points are selected; the calculated RMSE is 2.99 m, and the MAE is 2.11 m. In North Jutland, 1352 sampling points are used for validation, and the validation result presents an RMSE of 3.85 m and an MAE of 1.73 m. In Los Angeles, 200 sampling points are validated with an RMSE of 4.43 m and an MAE of 3.17 m. The three regions represent different dimensions, population densities, road network densities and road network topology characteristics. Therefore, our results are quite consistent with the reference road elevations for different regions with various road network characteristics. Overall, the RMSE between the estimated road node elevation and reference road node elevation is 3.80 m, and the MAE is 1.94 m. The estimated road elevation is consistent with the reference road elevation, and the slope of the regression line is close to 1. Figure 7 confirms the high reliability of our 3D road network dataset.

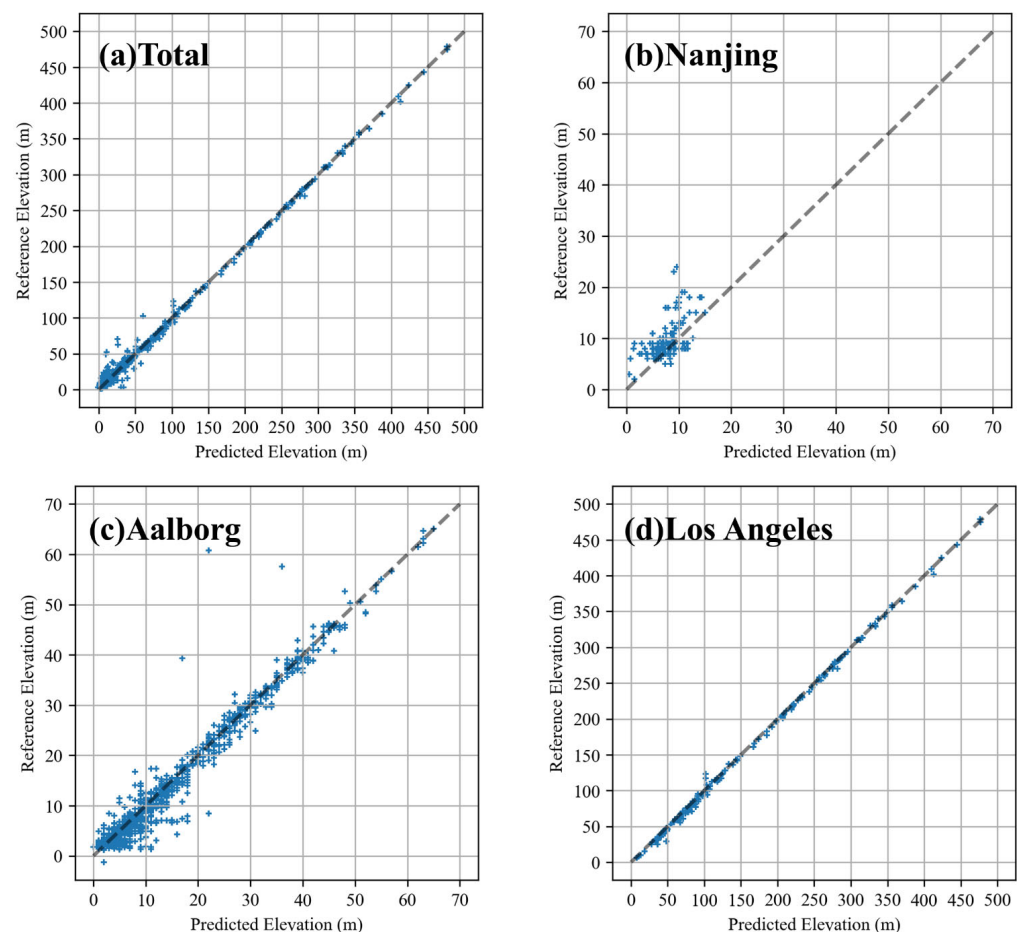


Figure 7. Road elevation validation with multi-source data (reference road elevation) in three regions. (a) Total of the three cities (b) Nanjing; (c) Aalborg; (d) Los Angeles.

4.2. Topology Assessment of Road Network

We also sample three interchanges of different scales and types in the three cities to check the correctness of their 3D topology (Figure 8). The types include cloverleaf, mixed and parclo. And the radii of the three 3D traffic projects are about 500, 200 and 100 m. We use remote sensing images and 3D visualization of the road network for comparison and validation. The three sample areas are located in a suburban area, a suburban junction and an inner-city area, which makes our assessment representative.

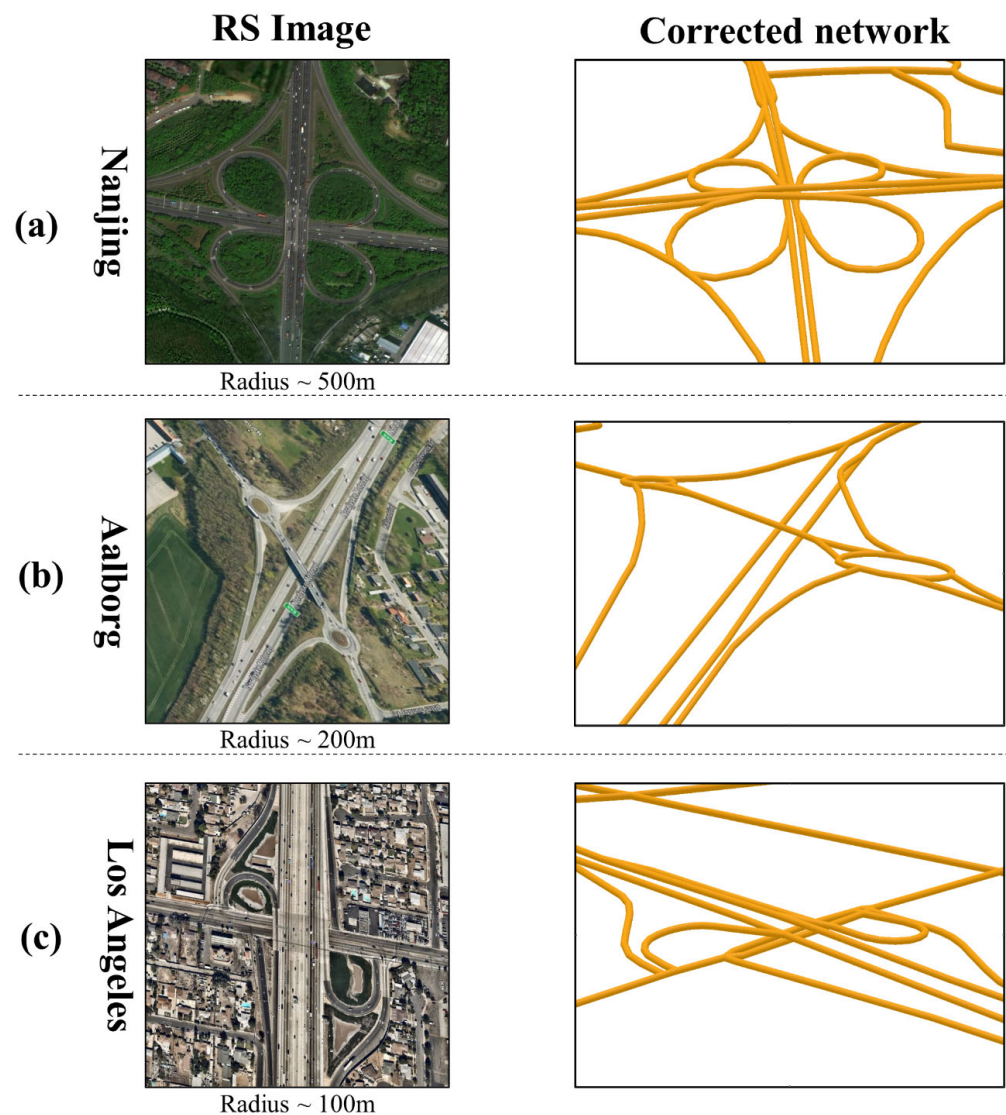


Figure 8. Road Topology validation with RS images in three interchanges of different radii. (a) Nanjing, radius about 500 m; (b) North Jutland, radius about 200 m; (c) Los Angeles, radius about 100 m.

The topology assessment is divided into two parts: the up-down relationship between the major roads and the up-down interconnection relationship of the approach roads. By visual interpretation, we find that the results have impressive performance on multiple radius scales. Specifically, the lower roads of interchanges are all in the correct spatial location in that they are below the upper roads, rather than intersecting as originally. Because the nodes between the main road and ramps were also preserved in the previous simplification steps, these nodes are corrected by multiple steps and the ramps link the upper and lower roads in the interchanges with the changes in end-node elevation.

Overall, the topological relationships between the upper and lower levels of the main roads and that of the upper and lower interconnections of the approach roads are correct, though some road nodes still contain noise and unnecessary undulations.

5. Discussion

5.1. Spatial Distribution of Road Edge Elevation and Absolute Grades

The spatial distribution of road edge average elevation in the three different regions is displayed in Figure 8. Unsurprisingly, most of the high average elevation of edges occurs in areas with higher elevations, in comparison with the FABDEM. Figure 9 also shows that the spatial pattern of average elevation presents consistency within the urban basement terrain, which indicates that our novel 3D road networks are valuable for large-scale urban studies.

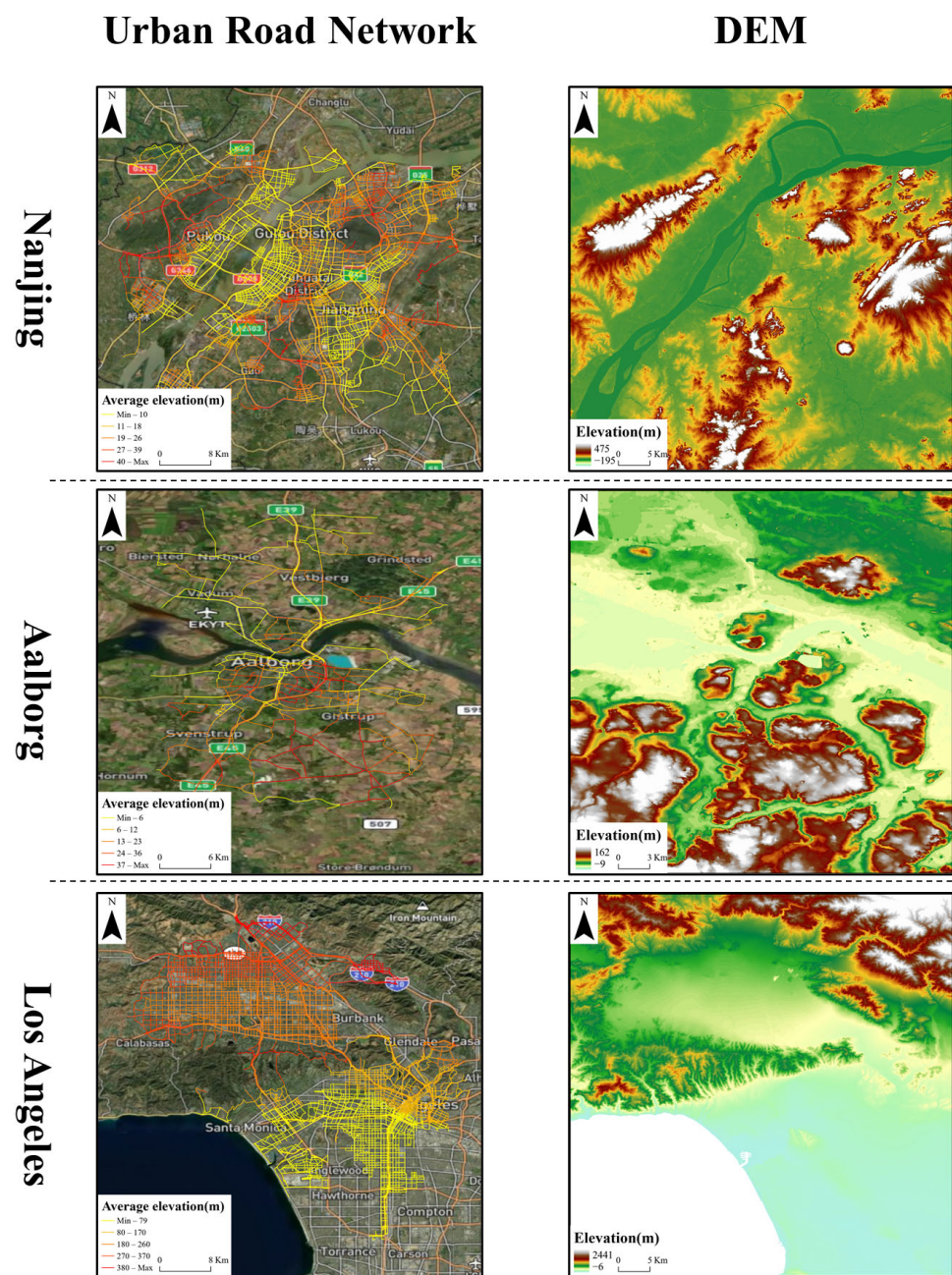


Figure 9. The average elevation of edges and DEM in three different areas.

Figure 10 shows the distribution of absolute grade differences between the uncorrected network and the correct network in Nanjing. The red line in the legend indicates that the absolute grades of edges are greater than 0.07, the maximum of grades in the road construction standards, whilst the blue line is the opposite. The result shows that the majority of edges with excessive absolute grades are corrected to less than 0.07.

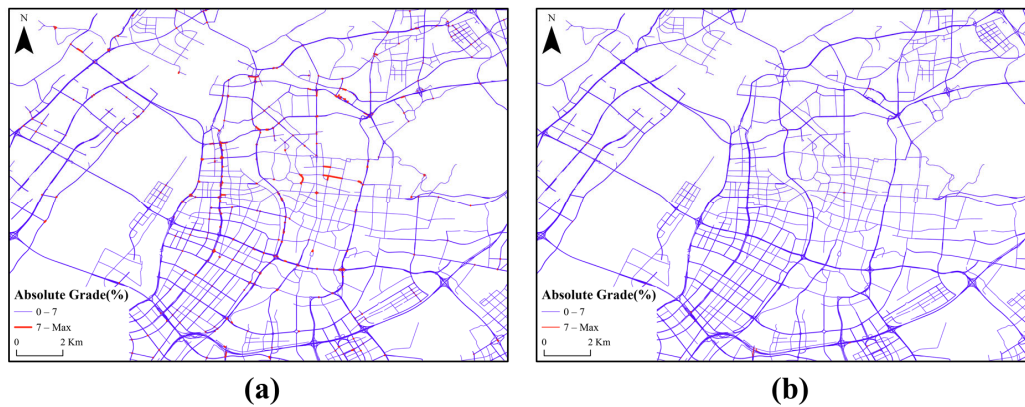


Figure 10. The spatial distribution of absolute grade (a) in the uncorrected road network; (b) in the corrected road network.

From a microscopic perspective, Figure 11 indicates our corrected result, compared to the original networks. The overestimated nodes near the high-rise buildings were corrected to appropriate values using surrounding building heights as references. It successfully demonstrates that our method eliminates most noise in the original result and corrects parts with untrustworthy nodes and edges at the centre of the city.

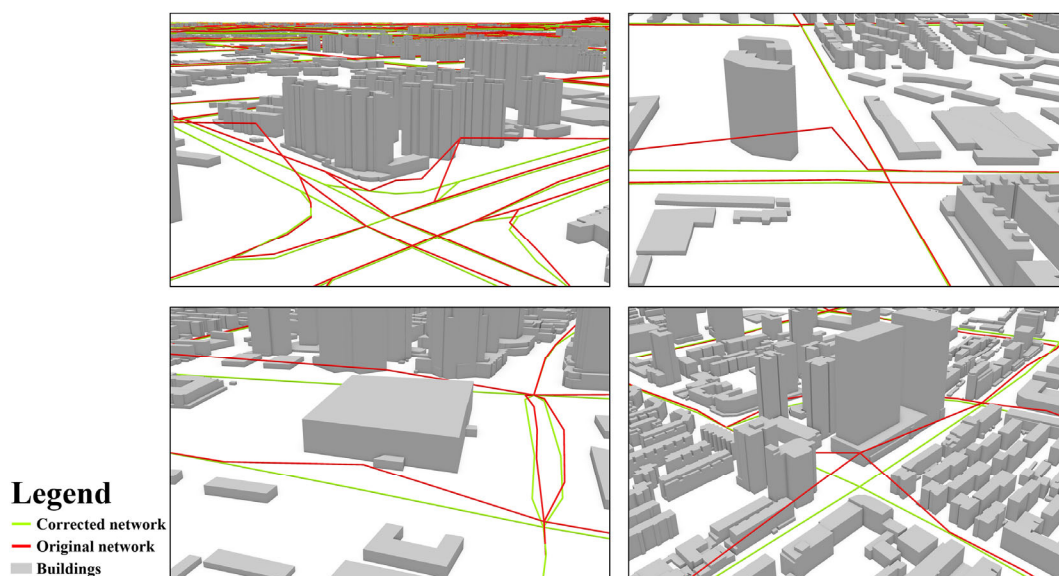


Figure 11. A comparison of corrected road network (green line) and original road (red line) in urban areas.

5.2. Potential Developing Directions

Our data sources have potential to be more reliable or replaced with other excellent data sources. Our generated 3D road network contains a small number of nonroad nodes because the position of nodes comes from various sources and presents uncertainty in OSM [59]. We fused multiple data for the correction work but incompletely ensured the reliability and consistent availability of data. For example, FABDEM is a new elevation data

source that has good performance in natural surfaces but has not been applied or verified in urban studies worldwide. Thus, obtaining a 2D road network with higher positioning accuracy and evaluating the accuracy of FABDEM data in urban areas are the next major problems to be solved. To fill data voids, AW3D30 DSM complements missing tiles in land areas with existing DEMs [47]. However, different data sources are produced using diverse instruments with their own elevation references, which leads to deviations within a city. In response, we are searching for some novel DSMs and DEMs from stereo images and interferometric SAR that have good performance in urban areas.

Our result has potential to be reconstructed more accurately. Some bridges over rivers were unable to be reconstructed in our result because most nodes of bridges were simplified and the elevation samples of bridges were ignored, which made us underestimate the elevation of bridges. Therefore, we plan to use the intersections of rivers and roads to identify the segments of bridges and reserve the nodes on the surface of bridges. This will help us reconstruct the bridges but will take considerable time. We also overestimated the height of tunnels in some road segments due to the inaccurate location marking in OSM, which caused a portion of the error.

Large-scale 3D road networks have the potential to be applied to 3D urban analysis. 3D road networks have elevation information and include 3D transportation facilities, such as viaducts and interchanges, especially, the roads in mountainous cities which may exhibit a height difference close to 10 m in a length of 100 m. Thus, the 3D characteristics of road networks should not be ignored and are worth further attention owing to their significance in 3D urban analysis. (1) As an indicator, the height difference of 3D road networks can be integrated with 2D topological factors to identify the urban functional zones [60], reveal the urban expansion phase [61] and indicate the spatial intercity and intracity heterogeneity [62]; (2) As data bases, 3D road networks can be applied to estimate the solar and wind energy potential [63,64], simulate the process of urban flood [65] and calculate the impact range of urban noise field [66] from a vertical perspective; (3) As a kind of unique urban facility, 3D road networks enrich the urban landscape [67], promote the quantitative study of urban morphology [68] and provide auxiliary information for urban landscape design and urban planning. For our data structures, the generated results including nodes and edges can be converted into directed graph structures. Compared with the format of shapefiles, they are not restricted to GIS software and meet the demands of other related analyses by deep learning or physical modelling.

6. Conclusions

In this study, we propose a 3D road network extraction method considering terrain and road engineering construction standards for large-scale projects, which fixes the nodes and edges with excessive grades in the original result, breaks through the shade of the upper road to the lower road in the interchanges and makes the 3D topological transportation features, such as tunnels and interchanges, more complete and in line with engineering standards. Furthermore, this method takes advantage of the complementary characteristics of multi-source datasets to deliver a complete, accurate and reliable road elevation dataset. Compared with existing methods, the 3D road network extraction method is applicable to large-scale studies and efficient without high hardware requirements. The final results of the extracted 3D road networks are compared with those of UAV DSM, LiDAR point cloud and Google Earth in three cities of different scales and development stages. The overall RMSE is 3.80 m, and the MAE is 1.94 m. Moreover, several interchanges with different radii are selected to test the reliability of the topology in this study, which proves that the 3D topology of the road network is generally correct.

There are still some deviations in the statistics of road elevations caused by rugged terrain and the uncertainty of the original data. Overall, this approach to extracting large-scale 3D road networks provides a new dimension for urban study. This is an essential supplement to the content of 3D cities. This model can be used for traffic congestion prediction, fuel consumption estimation and related 3D urban analysis.

We mainly use the OSMnx, NetworkX and GeoPandas [69] tools in our process, and the data structure is fully compliant with the OSM standard, which can be widely used in 3D road network-related research. The code is publicly available at https://github.com/CubicsYang/Road_Elevation_DSM (accessed on 2 November 2022).

Author Contributions: Conceptualization, Y.C. and X.Y.; methodology, Y.C., X.Y. and J.F.; validation, Y.C.; writing—original draft preparation, Y.C.; writing—review and editing, Y.C., X.Y. and L.Y.; visualization, Y.C. and L.Y.; software, Y.C.; supervision, X.Y.; funding acquisition, X.Y. All authors have read and agreed to the published version of the manuscript.

Funding: This research was funded by the National Natural Science Foundation of China (grant numbers 42171402, 41930102), the Priority Academic Program Development of Jiangsu Higher Education Institutions (number 164320H116).

Data Availability Statement: The data that support the findings of this study are available from the author upon reasonable request.

Acknowledgments: The authors express their gratitude to the journal editor and reviewers, whose thoughtful suggestions greatly contribute to improve the quality of this paper. Sincere gratitude is also given to Xingyu Zhou, Sijin Li and Hong Wei for their helpful comments on the manuscript.

Conflicts of Interest: The authors declare no conflict of interest.

References

1. Barthélemy, M. From Paths to Blocks: New Measures for Street Patterns. *Environ. Plan. B Urban Anal. City Sci.* **2017**, *44*, 256–271. [CrossRef]
2. Zhong, S.; Yang, X.; Chen, R. The accessibility measurement of hierarchy public service facilities based on multi-mode network dataset and the two-step 2SFCA: A case study of Beijing's medical facilities. *Geogr. Res.* **2016**, *35*, 731–744.
3. Kan, Z.; Tang, L.; Kwan, M.-P.; Ren, C.; Liu, D.; Li, Q. Traffic Congestion Analysis at the Turn Level Using Taxis' GPS Trajectory Data. *Comput. Environ. Urban Syst.* **2019**, *74*, 229–243. [CrossRef]
4. Herrera, J.C.; Work, D.B.; Herring, R.; Ban, X.; Jacobson, Q.; Bayen, A.M. Evaluation of Traffic Data Obtained via GPS-Enabled Mobile Phones: The Mobile Century Field Experiment. *Transp. Res. Part C Emerg. Technol.* **2010**, *18*, 568–583. [CrossRef]
5. Wang, H.; Zeng, W.; Cao, R. Simulation of the Urban Jobs–Housing Location Selection and Spatial Relationship Using a Multi-Agent Approach. *ISPRS Int. J. Geo-Inf.* **2021**, *10*, 16. [CrossRef]
6. Guo, Y.; Tang, Z.; Guo, J. Could a Smart City Ameliorate Urban Traffic Congestion? A Quasi-Natural Experiment Based on a Smart City Pilot Program in China. *Sustainability* **2020**, *12*, 2291. [CrossRef]
7. Zhou, Q.; Zhang, W. A Preliminary Review on 3-Dimensional City Model. In Proceedings of the Asia GIS 2003 Conference, Wuhan, China, 16–18 October 2003; pp. 16–18.
8. Ren, C.; Cai, M.; Li, X.; Shi, Y.; See, L. Developing a Rapid Method for 3-Dimensional Urban Morphology Extraction Using Open-Source Data. *Sustain. Cities Soc.* **2020**, *53*, 101962. [CrossRef]
9. Fang, Z.; Qi, J.; Fan, L.; Huang, J.; Jin, Y.; Yang, T. A Topography-Aware Approach to the Automatic Generation of Urban Road Networks. *Int. J. Geogr. Inf. Sci.* **2022**, *36*, 2035–2059. [CrossRef]
10. Badhrudeen, M.; Derrible, S.; Verma, T.; Kermanshah, A.; Furno, A. A Geometric Classification of World Urban Road Networks. *Urban Sci.* **2022**, *6*, 11. [CrossRef]
11. Fan, C.; Jiang, X.; Mostafavi, A. A Network Percolation-Based Contagion Model of Flood Propagation and Recession in Urban Road Networks. *Sci. Rep.* **2020**, *10*, 13481. [CrossRef]
12. Qing, Z.H.U.; Liguoz, Z.; Yulin, D.; Han, H.U.; Xuming, G.E.; Mingwei, L.I.U.; Wei, W. From Real 3D Modeling to Digital Twin Modeling. *Acta Geod. Cartogr. Sin.* **2022**, *51*, 1040.
13. Zhu, Q.; Li, Y. Hierarchical Lane-oriented 3D Road-network Model. *Int. J. Geogr. Inf. Sci.* **2008**, *22*, 479–505. [CrossRef]
14. Yeh, A.G.-O.; Zhong, T.; Yue, Y. Angle Difference Method for Vehicle Navigation in Multilevel Road Networks with a Three-Dimensional Transport GIS Database. *IEEE Trans. Intell. Transp. Syst.* **2017**, *18*, 140–152. [CrossRef]
15. Yang, L.; Yang, X.; Zhang, H.; Ma, J.; Zhu, H.; Huang, X. Urban Morphological Regionalization Based on 3D Building Blocks—A Case in the Central Area of Chengdu, China. *Comput. Environ. Urban Syst.* **2022**, *94*, 101800. [CrossRef]
16. Tavares, G.; Zsigraiová, Z.; Semião, V.; Carvalho, M. Optimisation of MSW Collection Routes for Minimum Fuel Consumption Using 3D GIS Modelling. *Waste Manag.* **2008**, *29*, 1176–1185. [CrossRef] [PubMed]
17. Guo, C.; Ma, Y.; Yang, B.; Jensen, C.S.; Kaul, M. Ecomark: Evaluating Models of Vehicular Environmental Impact. In Proceedings of the 20th International Conference on Advances in Geographic Information Systems, Redondo Beach, CA, USA, 7–9 November 2012; pp. 269–278.

18. Katzorke, N. Using RTK-Based Automated Vehicles to Pre-Mark Temporary Road Marking Patterns for Test Maneuvers of Automated Vehicles. In Proceedings of the 2022 International Conference on Connected Vehicle and Expo (ICCVE), Lakeland, FL, USA, 7–9 March 2022; pp. 1–5.
19. Yang, B.; Fang, L.; Li, J. Semi-Automated Extraction and Delineation of 3D Roads of Street Scene from Mobile Laser Scanning Point Clouds. *ISPRS J. Photogramm. Remote Sens.* **2013**, *79*, 80–93. [[CrossRef](#)]
20. Kaul, M.; Yang, B.; Jensen, C. Building Accurate 3D Spatial Networks to Enable Next Generation Intelligent Transportation Systems. In Proceedings of the 2013 IEEE 14th International Conference on Mobile Data Management, Milan, Italy, 3–6 June 2013; Volume 1.
21. Qian, C.; Gale, B.; Bach, J. Earth Documentation: Overpass Detection Using Mobile Lidar. In Proceedings of the 2010 IEEE International Conference on Image Processing, Hong Kong, China, 26–29 September 2010; IEEE: Piscataway, NJ, USA; pp. 3901–3904.
22. Gao, L.; Shi, W.; Zhu, J.; Shao, P.; Sun, S.; Li, Y.; Wang, F.; Gao, F. Novel Framework for 3D Road Extraction Based on Airborne LiDAR and High-Resolution Remote Sensing Imagery. *Remote Sens.* **2021**, *13*, 4766. [[CrossRef](#)]
23. Zhou, Y.; Huang, R.; Jiang, T.; Dong, Z.; Yang, B. Highway Alignments Extraction and 3D Modeling from Airborne Laser Scanning Point Clouds. *Int. J. Appl. Earth Obs. Geoinformat.* **2021**, *102*, 102429. [[CrossRef](#)]
24. McKenzie, G.; Janowicz, K. ISED: Constructing a High-Resolution Elevation Road Dataset from Massive, Low-Quality in-Situ Observations Derived from Geosocial Fitness Tracking Data. *PLoS ONE* **2017**, *12*, e0186474. [[CrossRef](#)]
25. Yang, Z.; Zhang, Q. Low-Cost and Accurate 3D Road Modeling Using Mobile Phone. *IEEE Trans. Mob. Comput.* **2016**, *15*, 2494–2506. [[CrossRef](#)]
26. Shu, J.; Wang, S.; Jia, X.; Zhang, W.; Xie, R.; Huang, H. Efficient Lane-Level Map Building via Vehicle-Based Crowdsourcing. *IEEE Trans. Intell. Transp. Syst.* **2022**, *23*, 4049–4062. [[CrossRef](#)]
27. Wang, J. Automatic High-Fidelity 3D Road Network Modeling. Ph.D. Thesis, Old Dominion University, Norfolk, VA, USA, 2011. [[CrossRef](#)]
28. Schpok, J. Geometric Overpass Extraction from Vector Road Data and DSMs. In Proceedings of the 19th ACM SIGSPATIAL International Conference on Advances in Geographic Information Systems; Association for Computing Machinery: New York, NY, USA, 2011; pp. 3–8.
29. Wang, Y.; Zou, Y.; Henrickson, K.; Wang, Y.; Tang, J.; Park, B.-J. Google Earth Elevation Data Extraction and Accuracy Assessment for Transportation Applications. *PLoS ONE* **2017**, *12*, e0175756. [[CrossRef](#)] [[PubMed](#)]
30. Li, L. 3D Road Network Extraction Method Based on UAV Oblique Photography. *China J. Highw. Transp.* **2019**, *32*, 219–226, 254.
31. Tachikawa, T.; Hato, M.; Kaku, M.; Iwasaki, A. Characteristics of ASTER GDEM Version 2. In Proceedings of the 2011 IEEE International Geoscience and Remote Sensing Symposium, Vancouver, BC, Canada, 24–29 July 2011; pp. 3657–3660.
32. Farr, T.G.; Rosen, P.A.; Caro, E.; Crippen, R.; Duren, R.; Hensley, S.; Kobrick, M.; Paller, M.; Rodriguez, E.; Roth, L. The Shuttle Radar Topography Mission. *Rev. Geophys.* **2007**, *45*, RG2004. [[CrossRef](#)]
33. Zhang, X.; Zhong, M.; Liu, S.; Zheng, L.; Chen, Y. Template-Based 3D Road Modeling for Generating Large-Scale Virtual Road Network Environment. *ISPRS Int. J. Geo-Inf.* **2019**, *8*, 364. [[CrossRef](#)]
34. Over, M.; Schilling, A.; Neubauer, S.; Zipf, A. Generating Web-Based 3D City Models from OpenStreetMap: The Current Situation in Germany. *Comput. Environ. Urban Syst.* **2010**, *34*, 496–507. [[CrossRef](#)]
35. Wang, H.; Wu, Y.; Han, X.; Xu, M.; Chen, W. Automatic Generation of Large-Scale 3D Road Networks Based on GIS Data. *Comput. Graph.* **2021**, *96*, 71–81. [[CrossRef](#)]
36. Tang, G.-A. Progress of DEM and Digital Terrain Analysis in China. *Acta Geogr. Sin.* **2014**, *69*, 1305–1325.
37. Xiong, L.; Li, S.; Tang, G.; Strobl, J. Geomorphometry and Terrain Analysis: Data, Methods, Platforms and Applications. *Earth-Sci. Rev.* **2022**, *233*, 104191. [[CrossRef](#)]
38. Santillan, J.R.; Makinano-Santillan, M. Vertical Accuracy Assessment of 30-M Resolution Alos, Aster, and Srtm Global Dems Over Northeastern Mindanao, Philippines. *Int. Arch. Photogramm. Remote Sens. Spat. Inf. Sci.* **2016**, *XLII-B4*, 149–156. [[CrossRef](#)]
39. Guth, P.L.; Geoffroy, T.M. LiDAR Point Cloud and ICESat-2 Evaluation of 1 Second Global Digital Elevation Models: Copernicus Wins. *Trans. GIS* **2021**, *25*, 2245–2261. [[CrossRef](#)]
40. Nikolakopoulos, K.G. Accuracy Assessment of ALOS AW3D30 DSM and Comparison to ALOS PRISM DSM Created with Classical Photogrammetric Techniques. *Eur. J. Remote Sens.* **2020**, *53*, 39–52. [[CrossRef](#)]
41. Stilla, U.; Soergel, U.; Thoennessen, U. Potential and Limits of InSAR Data for Building Reconstruction in Built-up Areas. *ISPRS J. Photogramm. Remote Sens.* **2003**, *58*, 113–123. [[CrossRef](#)]
42. Vargas-Munoz, J.E.; Srivastava, S.; Tuia, D.; Falcão, A.X. OpenStreetMap: Challenges and Opportunities in Machine Learning and Remote Sensing. *IEEE Geosci. Remote Sens. Mag.* **2021**, *9*, 184–199. [[CrossRef](#)]
43. Irshad, M.E.; Sohail, H.; Zafar, N.; Haq, I.U. A Framework for Synthesizing Tracker Speeds on Open Street Maps. In Proceedings of the 2020 IEEE 23rd International Multitopic Conference (INMIC), Bahawalpur, Pakistan, 5–7 November 2020; pp. 1–6.
44. Chakeri, A.; Wang, X.; Goss, Q.; Akbas, M.I.; Jaimes, L.G. A Platform-Based Incentive Mechanism for Autonomous Vehicle Crowdsensing. *IEEE Open J. Intell. Transp. Syst.* **2021**, *2*, 13–23. [[CrossRef](#)]
45. Boeing, G. OSMnx: New Methods for Acquiring, Constructing, Analyzing, and Visualizing Complex Street Networks. *Comput. Environ. Urban Syst.* **2017**, *65*, 126–139. [[CrossRef](#)]
46. Takaku, J.; Tadono, T.; Tsutsui, K. Generation of High Resolution Global DSM from ALOS PRISM. *Int. Arch. Photogramm. Remote Sens. Spat. Inf. Sci.* **2014**, *XL-4*, 243–248. [[CrossRef](#)]

47. Tadono, T.; Ishida, H.; Oda, F.; Naito, S.; Minakawa, K.; Iwamoto, H. Precise Global DEM Generation by ALOS PRISM. *ISPRS Ann. Photogramm. Remote Sens. Spat. Inf. Sci.* **2014**, *II-4*, 71–76. [[CrossRef](#)]
48. Huang, H.; Chen, P.; Xu, X.; Liu, C.; Wang, J.; Liu, C.; Clinton, N.; Gong, P. Estimating Building Height in China from ALOS AW3D30. *ISPRS J. Photogramm. Remote Sens.* **2022**, *185*, 146–157. [[CrossRef](#)]
49. Nonomura, A.; Hasegawa, S.; Kanbara, D.; Tadono, T.; Chiba, T. Topographic Analysis of Landslide Distribution Using AW3D30 Data. *Geosciences* **2020**, *10*, 115. [[CrossRef](#)]
50. Xu, Y.; Zhang, S.; Li, J.; Liu, H.; Zhu, H. Extracting Terrain Texture Features for Landform Classification Using Wavelet Decomposition. *ISPRS Int. J. Geo-Inf.* **2021**, *10*, 658. [[CrossRef](#)]
51. Hawker, L.; Uhe, P.; Paulo, L.; Sosa, J.; Savage, J.; Sampson, C.; Neal, J. A 30 m Global Map of Elevation with Forests and Buildings Removed. *Environ. Res. Lett.* **2022**, *17*, 024016. [[CrossRef](#)]
52. Marešová, J.; Gdulová, K.; Pracná, P.; Moravec, D.; Gábor, L.; Prošek, J.; Barták, V.; Moudrý, V. Applicability of Data Acquisition Characteristics to the Identification of Local Artefacts in Global Digital Elevation Models: Comparison of the Copernicus and TanDEM-X DEMs. *Remote Sens.* **2021**, *13*, 3931. [[CrossRef](#)]
53. OpenStreetMap contributors Planet Dump. 2017. Available online: <https://planet.osm.org> (accessed on 1 September 2022).
54. Hagberg, A.; Swart, P.; Chult, S.D. Exploring Network Structure, Dynamics, and Function Using Networkx. In *Proceedings of the SCIPY 08*; Pasadena, CA, USA, 21 August 2008, Los Alamos National Lab (LANL): Los Alamos, NM, USA, 2008.
55. American Association of State Highway and Transportation Official (AASHTO). *A Policy on Geometric Design of Highways and Streets 2018*, 7th ed.; American Association of State Highway and Transportation Officials: Washington, DC, USA, 2021.
56. *Technical Standard for Highway Engineering in Suburban and Rural Town Areas*; Ministry of Transport of the People’s Republic of China: Beijing, China, 2021.
57. California, S. of Highway Design Manual (HDM) | Caltrans. Available online: <https://dot.ca.gov/programs/design/manual-highway-design-manual-hdm> (accessed on 15 September 2022).
58. Wang, X.; You, S.; Wang, L. Classifying Road Network Patterns Using Multinomial Logit Model. *J. Transp. Geogr.* **2017**, *58*, 104–112. [[CrossRef](#)]
59. Girres, J.-F.; Touya, G. Quality Assessment of the French OpenStreetMap Dataset. *Trans. GIS* **2010**, *14*, 435–459. [[CrossRef](#)]
60. Liu, H.; Xu, Y.; Tang, J.; Deng, M.; Huang, J.; Yang, W.; Wu, F. Recognizing Urban Functional Zones by a Hierarchical Fusion Method Considering Landscape Features and Human Activities. *Trans. GIS* **2020**, *24*, 1359–1381. [[CrossRef](#)]
61. Burghardt, K.; Uhl, J.H.; Lerman, K.; Leyk, S. Road Network Evolution in the Urban and Rural United States since 1900. *Comput. Environ. Urban Syst.* **2022**, *95*, 101803. [[CrossRef](#)]
62. Xue, J.; Jiang, N.; Liang, S.; Pang, Q.; Yabe, T.; Ukkusuri, S.V.; Ma, J. Quantifying the Spatial Homogeneity of Urban Road Networks via Graph Neural Networks. *Nat. Mach. Intell.* **2022**, *4*, 246–257. [[CrossRef](#)]
63. Zhong, T.; Zhang, K.; Chen, M.; Wang, Y.; Zhu, R.; Zhang, Z.; Zhou, Z.; Qian, Z.; Lv, G.; Yan, J. Assessment of Solar Photovoltaic Potentials on Urban Noise Barriers Using Street-View Imagery. *Renew. Energy* **2021**, *168*, 181–194. [[CrossRef](#)]
64. Zahedi, R.; Ghorbani, M.; Daneshgar, S.; Gitifar, S.; Qezelbigloo, S. Potential Measurement of Iran’s Western Regional Wind Energy Using GIS. *J. Clean. Prod.* **2022**, *330*, 129883. [[CrossRef](#)]
65. Singh, P.; Sinha, V.S.P.; Vijhani, A.; Pahuja, N. Vulnerability Assessment of Urban Road Network from Urban Flood. *Int. J. Disaster Risk Reduct.* **2018**, *28*, 237–250. [[CrossRef](#)]
66. Rey Gozalo, G.; Suárez, E.; Montenegro, A.L.; Arenas, J.P.; Barrigón Morillas, J.M.; Montes González, D. Noise Estimation Using Road and Urban Features. *Sustainability* **2020**, *12*, 9217. [[CrossRef](#)]
67. Zeng, L.; Lu, J.; Li, W.; Li, Y. A Fast Approach for Large-Scale Sky View Factor Estimation Using Street View Images. *Build. Environ.* **2018**, *135*, 74–84. [[CrossRef](#)]
68. Huang, X.; Wang, Y. Investigating the Effects of 3D Urban Morphology on the Surface Urban Heat Island Effect in Urban Functional Zones by Using High-Resolution Remote Sensing Data: A Case Study of Wuhan, Central China. *ISPRS J. Photogramm. Remote Sens.* **2019**, *152*, 119–131. [[CrossRef](#)]
69. Jordahl, K.; den Bossche, J.V.; Fleischmann, M.; McBride, J.; Wasserman, J.; Richards, M.; Badaracco, A.G.; Gerard, J.; Snow, A.D.; Tratner, J.; et al. *Geopandas/Geopandas: V0.11.0* 2022. *Zenodo*. [[CrossRef](#)]